University of Ferrara
Mirco Andreotti
2002

Measurement of the Form Factor of the Proton for Large Time-like Momentum Transfers

Abstract

In the runII E835 has taken data at different energies corresponding to certain resonances of charmonium as shown in Tab.1:

State	M (MeV)	Γ (MeV)	Range of E_{CM} (MeV)	$\int Ldt$ (pb^{-1})
ψ'	3686	~ 277	$3666.0 \div 3704.0$	15.06
χ_0	3417	~ 9.8	$3340.0 \div 3470.0$	32.86
χ_1	3511	~ 0.88	$3509.6 \div 3511.7$	5.98
χ_2	3556	~ 2.0	$3535.0 \div 3557.9$	1.12
h_c	3526	< 1.1	$3523.3 \div 3528.9$	50.50
-	-	-	$3770.0 \div 3836.0$	5.17
-	-	-	$4267.0 \div 4270.0$	2.10

Table 1: Data taken by runII of E835.

The data at ψ' energy has been used to have a clean sample of events with e^+e^- in the final state. The search of form factor events is concentrated in the energy ranges out of the peak of χ_0 resonance, in this region there is a negligible contamination from $J/\psi\gamma$ decay; in the energy region at h_c, where the contamination from $J/\psi X$ is negligible; and in the two high energy regions, where there are not charmonium resonances. The data at the energy of χ_1 are not used because they are very near to the peak, while at the energy of χ_2 there are not events and the integrated luminosity is too low to estimate a good upper limit.

1 Introduction

The electromagnetic properties of the proton are parametrized by electric and magnetic form factors. In space-like ($q^2 < 0$) region electric and magnetic form factors of the proton have been measured in elastic electron-proton scattering up to $|q^2| = 10$ (GeV/c)^2 and $|q^2| = 31$ (GeV/c)^2 respectively. In time-like ($q^2 > 0$) region form factors of the proton have to be measured with annihilation processes, one way is to consider the reaction $\overline{p}p \to e^+e^-$. Since the cross section of this reaction contains electric and magnetic form factors, as shown in (1), from the selection of these events it is possible to measure the form factors.

$$\left(\frac{d\sigma}{d\Omega}\right)_{\overline{p}p\to e^+e^-} = \frac{\alpha^2}{4\beta_p s}\cdot\left[|G_M|^2\,(1+\cos^2\theta^*) + \frac{4m_p^2}{s}\,|G_E|^2\sin^2\theta^*\right] \tag{1}$$

Where θ^* is the scattering angle of the electron in c.m. and β_p is the speed of the proton(antiproton) in c.m.: $\beta_p = \sqrt{1-4m_p^2/s}$.
The region near threshold up to $s \sim 5$ GeV^2 is well studied, while at high energies only two experiments have measured the form factor of the proton: the first is E760 at Fermilab with three point at s =8.9, 12.4 and 13.0 GeV^2; the second is E835 runI at Fermilab with five point at s =8.8, 10.78, 12.4, 13.11 and 14.36 GeV^2 and an upper limit at s =18.4 GeV^2.
In this paper we present the results from runII(2000) of the experiment E835 at Fermilab in the energy range 3.3 GeV $< \sqrt{s} <$ 4.3 GeV.

2 Experimental apparatus

To be written.

3 Trigger and event selection

We need a selection with a high rejection factor to extract events with e^+e^- in the final state, which are characterized by a cross section of few pb to be compared with the $\overline{p}p$ total cross section of $\sim$ 60 mb.

The first level trigger for the e^+e^- final state requires the two electrons: each defined as the coincidence of the appropriate elements of H1, H2 and the corresponding cells of the Čerenkov . Independently the first level trigger requires two high-energy showers in the central calorimeter with an azimuthal opening angle greater than 90^o.

Events which satisfy the first level trigger are processed by the on-line filter, which, check events, in which the two highest-energy clusters in CCAL have an invariant mass greater than 2.2 GeV/c^2.

To reduce the recorded data we apply a preselection, which uses the same variables that we will use in the final selection. In the following discussion we show the variables and criteria used in the preselection and in the final selection. Each event is reconstructed off-line using all information by inner detector, Čerenkov counter and Central Calorimeter. The two electron candidates are identified as the tracks with the highest invariant mass.
The selection of $\overline{p}p \to e^+e^-$ proceeds in four steps.

(a) *Electron identification.* For each candidate electron track a variable is constructed, called *Electron Weight* (*EW*), using the pulse heights in H1, H2, H2' and Čerenkov counter, second moments of the transverse shower distribution in CCAL and the fractional shower energy in 3×3 block region of CCAL. *EW* is a likelihood ratio for the electron hypothesis versus background hypothesis. Since we search events with two electron we use the product of the two *Electron Weights.* It is reported in Fig. 1 an example of distribution of $\log_{10}(ew1 * ew2)$ for a sample of events at ψ' energy and for background. The preselection requires that $\log_{10}(ew1 * ew2) > -1$, it is also required an invariant mass of the two candidate electrons grater than 2.2 GeV/c^2. In the final selection we require $\log_{10}(ew1 * ew2) > 0$.

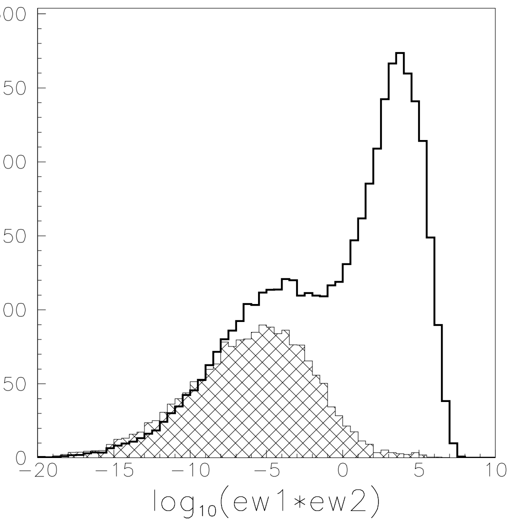

Figure 1: Distribution of $\log_{10}(ew1 * ew2)$ for a sample of data at ψ' energy (white) and for background events selected at $s = 14.40$ GeV^2 (cross-hatched). Both samples satisfy first level trigger, online filter and the request $M_{e^+e^-} > 2.6$ GeV (invariant mass of two most energetic clusters in CCAL).

(b) *Fiducial volume.* To ensure homogeneities in the response of the detector we accept only events in which the two electron have polar angles in the interval $15^o < \theta < 60^o$. This region is well covered by Central Calorimeter, Čerenkov counter and inner detector.

(c) *CCAL multiplicity.* To avoid rejecting events in which the electron or positron radiates a Bremsstrahlung photon which forms a distinct cluster in the CCAL, we do not impose a strict cut demanding only two ontime clusters. Events with more than two ontime clusters are kept provided that the extra clusters, when paired with either electron candidate, give an invariant mass below 100 MeV/c^2. In addition any number of out-of-time or undetermined clusters is allowed.

(d) *Kinematic fit.* The goodness of the e^+e^- final state is finally tested by means of a four constraint kinematics fit. Since the energy range considered is near to charmonium resonances which decay into $J/\psi X$ we use also a kinematic fit to test $J/\psi X$ final state, then we compare the fit probability for e^+e^- ($Prb(e^+e^-)$) with that for $J/\psi X$ ($Prb(J/\psi X)$). The events is accepted if $Prb(e^+e^-) > Prb(J/\psi X)$ and if $Prb(e^+e^-) > 1\%$.

In summary, the final selection consists of the following cuts:

$$\log_{10}(ew1 * ew2) > 0 \tag{2}$$

$$Fiducial\ volume \tag{3}$$

$$e^+e^- ontime \tag{4}$$

$$\forall\ extra\ cluster\ ontime\ [M_{\gamma e_1} \leqslant 100 \text{ MeV}] \text{ or } [M_{\gamma e_2} \leqslant 100 \text{ MeV}] \tag{5}$$

$$[Prb(e^+e^-) > Prb(J/\psi X)] \text{ and } [Prb(e^+e^-) > 1\%] \tag{6}$$

The final selection characterized from the above cuts is stable [1].

[1] See Appendix C for more details.

In the Tab. 2 are reported the energy regions used for the form factor selection and the number of selected form factor events.

Sample	$\sqrt{s}$ Interval (GeV)	Mean±Rms (GeV)	L (pb^{-1})	N
1	3.340-3.392	3.379±0.014	8.52	8
2	3.430-3.470	3.455±0.019	3.95	3
3	3.523-3.529	3.526±0.006	50.50	31
4	3.770-3.836	3.795±0.050	5.17	0
5	4.267-4.270	4.268±0.002	2.10	0

Table 2: Summary of data used for the form factor analysis.

4 Efficiencies

The overall efficiency of the analysis is the product of the three efficiencies corresponding to the first level trigger, the off-line preselection and the final selection. The efficiency of the on-line filter is practically one.

In order to calculate these efficiencies we used a clean sample of $\psi' \to e^+e^-$ events selected with different tight cuts, which depend from which efficiency we are considering.

The trigger efficiency ϵ_{trig} has been calculated from special trigger runs at the ψ' energy, which required only one electron [2]. The trigger efficiency turns out to be [1]:

$$\epsilon_{trig}^{data} = 0.90 \pm 0.02 \tag{7}$$

The efficiency of the preliminary selection has been calculated with four clean samples of $\psi' \to e^+e^-$ events selected requiring only two ontime cluster and applying tight topological cuts relative to the two body final state. The value of the efficiency obtained from these samples is [3]:

$$\epsilon_{pres}^{data} = 0.966 \pm 0.013(stat)^{+0.027}_{-0.036}(syst) \tag{8}$$

To estimate the efficiency of the final selection we considered the events selected at ψ' formation energy. The efficiency of the restriction on the fiducial volume will be taken into account in the integration of the differential cross section (1).

Fig.2 shows invariant mass distribution for candidate electron after preliminary selection (a) and after final selection (b) at the ψ' formation energy. The cross-hatched areas in both histograms correspond to the background contamination in these samples, extracted applying the same analysis to the data taken off resonance at $\sqrt{s} = 3.7$ GeV. Horizontal lines correspond to the decay $\psi' \to J/\psi X$ selected requiring $Prb(J/\psi X) > 1\%$ and $Prb(e^+e^-) < 10\%$ (with an efficiency of $\sim 95\%$). It can be seen that the background contamination from J/ψ-inclusive decay is very low.

[2] With special trigger runs an integrated luminosity of 0.99 nb^{-1} has been collected.

[3] See Appendix B for more details.

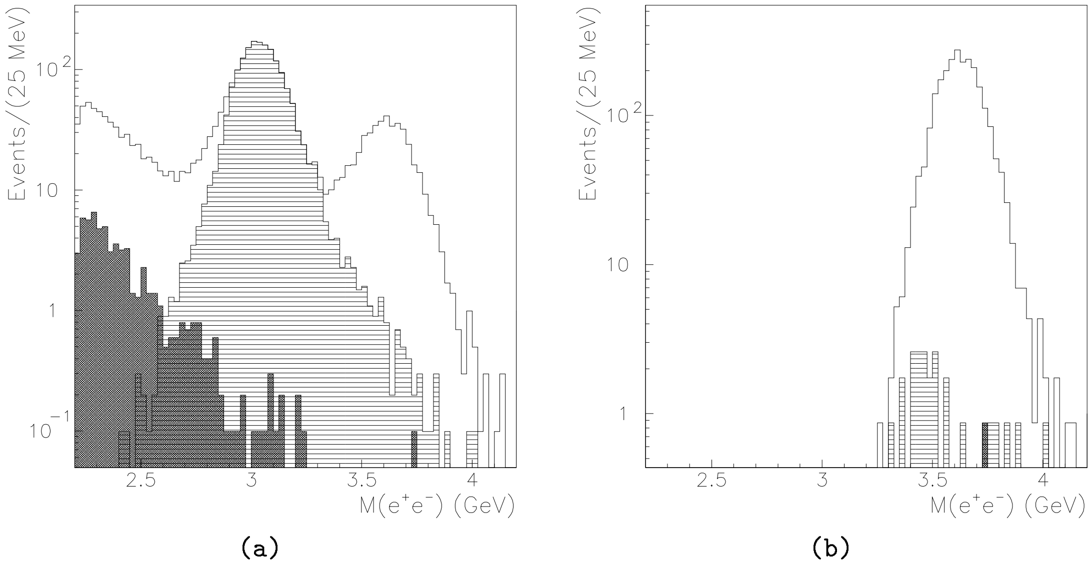

Figure 2: Invariant mass distribution for candidate electrons after preliminary selection (a) and after final selection (b): at ψ' energy (white) and at $\sqrt{s} = 3.7$ GeV (cross-hatched); horizontal lines correspond to J/ψ-inclusive subsample at ψ' energy. (The number of events has been rescaled by luminosity).

The efficiency of the final selection is defined as the fraction of events in the preliminary sample (Fig.2(a) white) that survive all cuts (Fig.2(b) white), once background (including $J/\psi X$ events) is subtracted. We consider only the events with invariant mass grater than 3.4 GeV.
The efficiency of the final selection is:

$$\epsilon_{sel} = 0.679 \pm 0.009(stat)^{+0.037}_{-0.026}(syst) \tag{9}$$

then the overall efficiency of the analysis is:

$$\epsilon_{ana} = 0.590 \pm 0.017(stat)^{+0.036}_{-0.032}(syst) \tag{10}$$

5 Studies of background reaction

The background reactions which can simulate the same signal of e^+e^- final state are inclusive $J/\psi X$ events, photon conversions, π^0 Dalitz decays and two body hadronic final states (mainly $\pi^+\pi^-$). The contributions from these background sources have been estimated with the same method used with data of runI of E-835 [3].

Inclusive $J/\psi X$

Above a certain threshold, the process $\overline{p}p \to J/\psi X$ followed by $J/\psi \to e^+e^-$ can fit the e^+e^- two body kinematics, when X is not detected. Since in the final selection we allow bremsstrahlung photons, near to the energy of χ_0 there is a decay which could satisfy the final selection:

$$\overline{p}p \to \chi_0 \to J/\psi\gamma \tag{11}$$

Considering the 10 events selected with form factor analysis at the peak [4] of χ_0 as due to $J/\psi\gamma$ decay, we rescale with Breit-Wigner formula and we find that at $s = 11.42$ GeV^2 and at $s = 11.93$ GeV^2 the cross section of process $\chi_0 \rightarrow J/\psi\gamma$ that survive at form factor analysis assume the values reported in Tab.6.
At the formation energy of h_c the contamination from inclusive $J/\psi X$ could come from the decay of this resonance into $J/\psi\pi^0$, then we define the background cross section from this contamination as:

$$\sigma^{'}_{J/\psi X}(s = 12.43 \text{ GeV}^2) = \alpha \times \sigma(\overline{p}p \rightarrow J/\psi\pi^0) \tag{12}$$

where α is the probability, for an inclusive event, of satisfying two-body kinematics. This probability has been evaluated at the χ_1 resonance, in $J/\psi\gamma$ decays in which the photon is not detected, selected requiring $Prb(J/\psi X) > 1\%$, $Prb(e^+e^-) < 10\%$ and only two clusters. $\alpha = 10^{-3}$ is the fraction of events which satisfy the two body kinematics fit probability cut. The value of $\sigma(\overline{p}p \rightarrow J/\psi\pi^0)$ is less than 5 pb [4]. The background contribution from inclusive events at 12.43 GeV^2 is less than 1.5×10^{-3} pb, as reported in Tab.6. The same upper limit is used at 14.40 GeV^2 and 18.22 GeV^2.

Photon conversions and Dalitz decays

The conversion in matter of a photon ($\gamma \rightarrow e^+e^-$) and Dalitz decay of a π^0 ($\pi^0 \rightarrow e^+e^-\gamma$) could contribute with a signal like that of the e^+e^- final state. The processes which contribute at this background are:

$$\overline{p}p \rightarrow \pi^0\pi^0 \tag{13}$$

$$\overline{p}p \rightarrow \pi^0\gamma \tag{14}$$

$$\overline{p}p \rightarrow \gamma\gamma \tag{15}$$

From reaction (15) if both photons convert in matter, a back-to-back electron-positron pair could simulate an e^+e^- signal. Also the other two reactions can generate a a back-to-back electron-positron pair by two different decays of π^0: the pion decays into two photons one of which or both convert in matter; the pion undergoes Dalitz decay.

The expected background cross section due to processes (13), (14) and (15) is:

$$\sigma_p < \omega \left[(\delta + 2\eta)^2 \sigma^{'}_{\pi^0\pi^0} + (\delta + 2\eta)\eta\sigma^{'}_{\pi^0\gamma} + \eta^2\sigma_{\gamma\gamma} \right] \tag{16}$$

where η is the probability of a photon to convert in matter before H1 and it has been calculated to be $\eta < 1.7 \times 10^{-2}$ from a clean sample of $\overline{p}p \rightarrow \pi^0\pi^0$ events [5]; $\delta = 1.2 \times 10^{-2}$ is the probability of a pion to decay through the Dalitz process; ω is the probability that a background event with two back-to-back charged tracks satisfy the cut $\log_{10}(ew1 * ew2) > 0$. This probability has been estimated on a sample of "pairs", defined as charged tracks with a large energy deposit in the CCAL that, combined with another calorimeter cluster, give a π^0 invariant mass. The result is $\omega = 10^{-2}$.
Finally, $\sigma^{'}_{\pi^0\pi^0}$ and $\sigma^{'}_{\pi^0\gamma}$ are, the feed-down background from $\pi^0\pi^0$ and $\pi^0\gamma$ to $\gamma\gamma$ respectively; they have been estimated in E760 with Monte Carlo techniques [8] (Tab.3).

[4]Around the peak of χ_0 we have considered the energy range: $M_{\chi_0} - \frac{\Gamma_{\chi_0}}{2} \leqslant E_{cm} \leqslant M_{\chi_0} - \frac{\Gamma_{\chi_0}}{2}$, with $L = 11.07$ pb^{-1}.

[5]See Appendix D for detailed description of the selection of these events and for the calculation of η.

$\sqrt{s}$ (GeV)	$\sigma'_{\pi^0\pi^0}+\sigma'_{\pi^0\gamma}$ (nb)	$\sigma_{\gamma\gamma}$ (nb)
11.42	1.6×10^{-1}	2.0×10^{-1}
11.93	1.0×10^{-1}	1.5×10^{-1}
12.43	0.9×10^{-1}	1.0×10^{-1}
14.40	$<0.4\times10^{-1}$	$<0.9\times10^{-1}$
18.22	$<0.4\times10^{-1}$	$<0.9\times10^{-1}$

Table 3: $\sigma'_{\pi^0\pi^0}+\sigma'_{\pi^0\gamma}$: cross section for $\pi^0\pi^0$ or $\pi^0\gamma$ final states simulating $\gamma\gamma$, based upon E-760 data and Monte Carlo calculation [8]. $\sigma_{\gamma\gamma}$: total cross section measured from E-760 data [8]. The last two upper limits has been evaluated at the ψ' formation energy. The cross sections have been calculated integrating differential cross sections over E835 fiducial volume.

Numerically, σ_p ranges from 3.1×10^{-3} pb at 11.42 GeV^2 to 1.7×10^{-3} pb at 12.43 GeV^2, as shown in Tab.6.

The cross sections $\sigma'_{\pi^0\pi^0}$, $\sigma'_{\pi^0\gamma}$ and $\sigma_{\gamma\gamma}$ have been calculated also in E835 runI [9], but over a limited angular coverage ($|\cos\theta^*|<0.40\div0.45$). In order to see how the E760 and E835(I) data compare, we have calculated the E760 cross sections integrated over the E835 angular range. The comparison is reported in Tab.4, from which we see that the E760 and E835(I) values differ by $\approx 25\%$, with the E835(I) values consistently lower. For the calculation of the background from photon conversion and Dalitz decay we have therefore decided to use the E760 cross sections integrated over E835 fiducial volume (the upper limits $|\cos\theta^*|_{max}$ have been taken from Tab.7).

E_{CM} (MeV)	$\sigma'_{\pi^0\pi^0}+\sigma'_{\pi^0\gamma}$ (pb)		$\sigma_{\gamma\gamma}$ (pb)	
	E760	E835(I)	E760	E835(I)
3526	25	20	28	21
3686	16	11	22	12

Table 4: Comparison of the cross section $\sigma'_{\pi^0\pi^0}$, $\sigma'_{\pi^0\gamma}$ and $\sigma_{\gamma\gamma}$ calculated in E835(I) [9] with those calculated in E760 [8] and integrated in the same angular region ($|\cos\theta^*|<0.45$).

Hadronic two-body

The most relevant source of background two body final state comes from the reaction:

$$\overline{p}p \rightarrow \pi^+\pi^- \tag{17}$$

The high cross section of this process and the high velocity of the pions are the causes of a possible signal in the Čerenkov counter and of an hadronic shower in CCAL with the characteristics of an electromagnetic shower, which could simulate $\overline{p}p \rightarrow e^+e^-$.
The expected background cross section from reaction (17) is:

$$\sigma_h = (\alpha_{acc}\times\sigma_{\pi^+\pi^-})\times\xi^2\times k^2 \tag{18}$$

where $\alpha_{acc}\times\sigma_{\pi^+\pi^-}$ is the cross section for reaction(17) integrated on the fiducial volume of the E-835 apparatus, whose values are reported in Tab.5 [5][6][7]; ξ is the probability that a pion generate a hadronic shower in CCAL with an energy compatible with the e^+e^- hypothesis; k is the probability that a pion releases a number of photoelectrons in the Čerenkov compatible with the Electron-Weight cut used in the preselection. These two probabilities have been measured from a sample of $\overline{p}p \rightarrow \pi^+\pi^-$ events collected with a special trigger, which required two hadron. The result is [6]: $\xi = 10^{-2}$; $k = 6 \times 10^{-3}$.

$\sqrt{s}$ (GeV)	$\alpha_{acc}\sigma_{\pi^+\pi^-}$ (nb)
11.42	1.5
11.93	1.0
12.43	0.8
14.40	< 0.2
18.22	< 0.2

Table 5: $\overline{p}p \rightarrow \pi^+\pi^-$ cross section integrated over E835 fiducial volume, taken from literature [5][6][7]. The last two upper limits has been evaluated at the ψ' formation energy.

The numerical values of σ_h range from 4.3×10^{-3} at 11.42 GeV^2 to 2.9×10^{-3} at 12.43 GeV^2.

The various background contributions are summarized in Tab.6. By adding them up we obtain the upper limits σ_B.

s (GeV^2)	$\sigma_{J/\psi X}$ (pb)	σ_p (pb)	σ_h (pb)	σ_B (pb)
11.42	3.0×10^{-2}	3.1×10^{-3}	4.3×10^{-3}	3.7×10^{-2}
11.93	2.3×10^{-2}	2.0×10^{-3}	3.6×10^{-3}	2.9×10^{-2}
12.43	1.5×10^{-2}	1.7×10^{-3}	2.9×10^{-3}	2.0×10^{-2}
14.40	$< 1.5 \times 10^{-2}$	$< 0.9 \times 10^{-3}$	$< 0.7 \times 10^{-3}$	$< 1.7 \times 10^{-2}$
18.22	$< 1.5 \times 10^{-2}$	$< 0.9 \times 10^{-3}$	$< 0.7 \times 10^{-3}$	$< 1.7 \times 10^{-2}$

Table 6: Expected background cross section from inclusive $J/\psi X$ reaction ($\sigma_{J/\psi X}$), photon conversions (σ_p) and from $\pi^+\pi^-$ final state (σ_h). σ_B is the total background cross section.

Comparing the estimated upper limits with the values of cross section reported in Tab.7 we can consider the background contamination negligible, therefore no subtraction from the number of candidate events is performed.

6 Measurement of the magnetic form factor of the proton

The number of events N selected with an integrated luminosity L and an efficiency ϵ allow us to calculate the differential cross section integrated in the c.m. acceptance region as follow:

$$\sigma_{acc} = \frac{N}{\epsilon L} \tag{19}$$

[6]See Appendix E for a detailed description of the selection of $\overline{p}p \rightarrow \pi^+\pi^-$ and of the evaluation of the two rejection powers.

σ_{acc} is a function of the magnetic and electric form factors G_M and G_E:

$$\begin{aligned}\sigma_{acc} &= \int_0^{2\pi} d\phi \int_{-|\cos\theta^*|_{max}}^{+|\cos\theta^*|_{max}} \frac{d\sigma}{d\Omega} d(\cos\theta^*) \\ &= \frac{\pi\alpha^2}{2\beta_p s} \cdot \left[A \cdot |G_M|^2 + \frac{4m_p^2}{s} \cdot B \cdot |G_E|^2 \right]\end{aligned} \tag{20}$$

where A and B are:

$$A = 2 \cdot \int_0^{+|\cos\theta^*|_{max}} (1 + \cos^2\theta^*) d(\cos\theta^*) \tag{21}$$

$$B = 2 \cdot \int_0^{+|\cos\theta^*|_{max}} (1 - \cos^2\theta^*) d(\cos\theta^*) \tag{22}$$

At different values of s the fiducial volume $15^o < \theta < 60^o$ corresponds to different acceptance regions for θ^*. At $\sqrt{s} < 3.661$ GeV, it is an upstream edge of the fiducial range ($\theta = 60^o$) that determines $|\cos\theta^*|_{max}$; whereas for $\sqrt{s} > 3.661$ GeV it is a downstream edge ($\theta = 15^o$) that constrains the acceptance.
Since the small number of events and the limited $\cos\theta^*$ range do not allow us to measure the angular distribution, two alternative hypotheses have been made: (a) $|G_E| = |G_M|$, as at the threshold of the timelike region ($s = 4m_p^2c^4$); (b) the "electric" contribution is assumed to be negligible. Under these two hypotheses the expressions of $|G_M|$ are respectively:

$$(a) \quad |G_M| = \left[\frac{2\ \beta_p\ s\ N}{\pi\ \alpha^2\ \left[A + \frac{4m_p^2}{s} B\right]\ L\ \epsilon} \right]^{\frac{1}{2}} \tag{23}$$

$$(b) \quad |G_M| = \left[\frac{2\ \beta_p\ s\ N}{\pi\ \alpha^2\ A\ L\ \epsilon} \right]^{\frac{1}{2}} \tag{24}$$

Tab.7 shows the results of the magnetic form factor of the proton calculated with the two hypotheses.

Quantum Chromodinamics predicts an asymptotic behavior for the magnetic form factor of the proton in the timelike region at high energy of the form:

$$G_M(Q^2) = \frac{C}{s^2} \cdot \left(\ln \frac{s}{\Lambda^2} \right)^{-2} \tag{25}$$

where C and Λ are two free parameters, which can be determined from measured values of the form factor.
Fitting the eleven values of the magnetic form factor determined from the experiments E760 [28], E835(I) [29] and E835(II) (this analysis), reported in Tab. 8 and plotted in Fig. 3, we obtain the following values of the parameters:

$$\begin{aligned} C &= 17^{+17}_{-7} \\ \Lambda &= 0.85^{+0.30}_{-0.36} \\ \chi^2/ndf &= 0.1 \end{aligned}$$

While fitting all 32 existing values (reported in Fig. 4) of the magnetic form factor in timelike region we obtain the following parameters:

$$C = 57^{+12}_{-9}$$
$$\Lambda = 0.30 \pm 0.05$$
$$\chi^2/ndf = 1.7$$

s (GeV^2)	L (pb^{-1})	N	σ_{acc} (pb)	$\vert\cos\theta^*\vert_{max}$	$10^2 \times \vert G_M\vert$ (a)	$10^2 \times \vert G_M\vert$ (b)
11.42±0.09	8.52	8	$1.64^{+0.81+0.11}_{-0.57-0.10}$	0.568	$1.74^{+0.43+0.06}_{-0.30-0.05}$	$1.95^{+0.48+0.07}_{-0.34-0.05}$
11.93±0.13	3.95	3	$1.33^{+1.29+0.09}_{-0.72-0.08}$	0.585	$1.59^{+0.77+0.06}_{-0.43-0.05}$	$1.77^{+0.86+0.06}_{-0.48-0.06}$
12.43±0.01	50.50	31	$1.07^{+0.23+0.07}_{-0.20-0.07}$	0.601	$1.45^{+0.15+0.05}_{-0.13-0.04}$	$1.60^{+0.17+0.06}_{-0.15-0.05}$
14.40±0.19	5.17	0	< 0.85	0.603	< 1.42	< 1.56
18.22±0.01	2.10	0	< 2.10	0.512	< 2.85	< 3.08

Table 7: Summary of the results of the form factor analysis using real efficiency. $\sigma_{acc} = N/(\epsilon \cdot L)$; $|\cos\theta^*|_{max}$ is the maximum value of $|\cos\theta^*|$ where θ^* is the scattering angle in c.m.; (a) $|G_M|$ calculated in the hypothesis $|G_E| = |G_M|$; (b) $|G_M|$ calculated in the approximation of negligible electric contribution.

s (GeV^2)	$10^2 \times \|G_M\|$	N	Experiment	Year
8.84±0.16	$3.59^{+0.18}_{-0.19}$	93	E-835(I)[29]	1999
8.9	$3.3^{+0.6}_{-0.4}$	14	E-760[28]	1993
10.78±0.28	$2.13^{+0.70}_{-0.84}$	3	E-835(I)[29]	1999
11.42±0.09	$1.74^{+0.43}_{-0.30}$	8	E-835(II)	2001
11.93±0.13	$1.59^{+0.77}_{-0.43}$	3	E-835(II)	2001
12.4	$1.3^{+0.3}_{-0.2}$	11	E-760[28]	1993
12.43±0.02	$1.43^{+0.12}_{-0.13}$	33	E-835(I)[29]	1999
12.43±0.01	$1.45^{+0.15}_{-0.13}$	38	E-835(II)	2001
13.0	$1.3^{+0.5}_{-0.3}$	4	E-760[28]	1993
13.11±0.18	1.12 ± 0.16	14	E-835(I)[29]	1999
14.36±0.50	$1.39^{+0.91}_{-0.54}$	1	E-835(I)[29]	1999

Table 8: Values of the magnetic form factor calculated with the hypothesis $|G_E| = |G_M|$ plotted in Fig. 3.

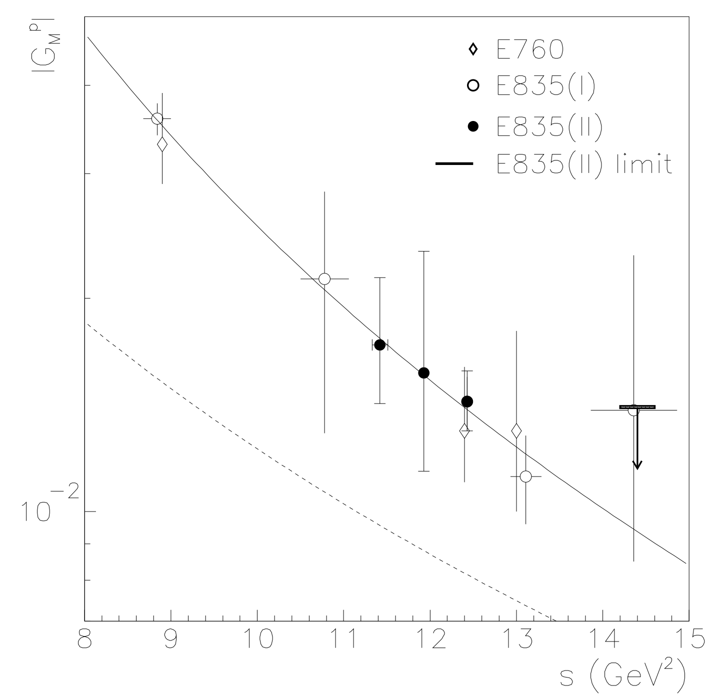

Figure 3: Fit of the form factor with the function (25) (solid line) from which we obtain the following parameter: $C = 18^{+18}_{-7}$ GeV^4, $\Lambda = 0.85^{+0.30}_{-0.36}$ GeV and $\chi^2/ndf = 0.1$. ($\diamond$) data of E760[28]; ($\circ$) data of E835(I)[29]; ($\bullet$) data of E-835(II). Also shown is the dipole (dashed line) behavior of the form factor in spacelike region. It is also plotted one of the two upper limit estimated in this analysis (90% CL). E835(II) results are obtained with the hypothesis (a).

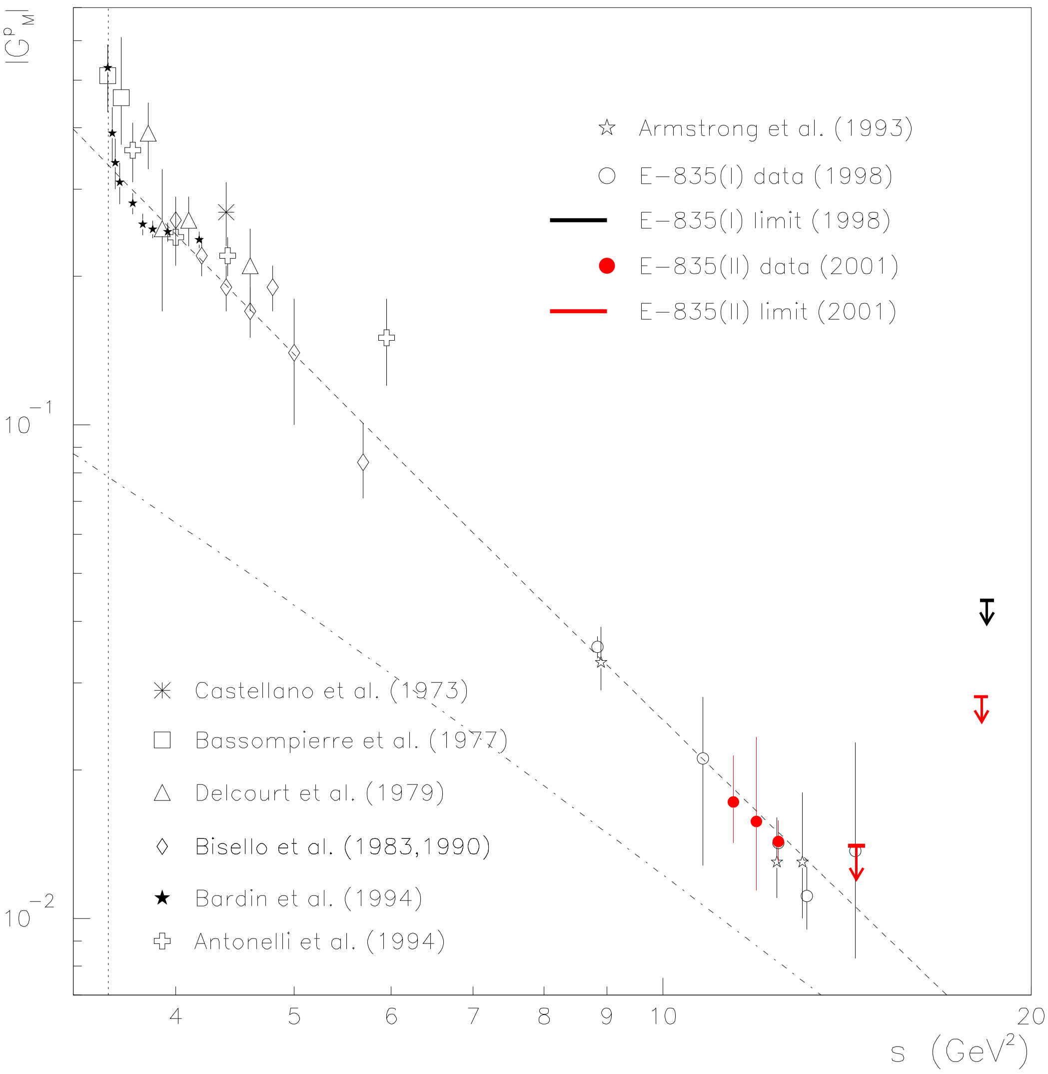

Figure 4: All existing values of the magnetic form factor in timelike region obtained with the hypothesis $|G_M| = |G_E|$. Upper limits are evaluated at 90% CL. We have also shown the asymptotic behavior in timelike region (solid line), dipole behavior in spacelike region (line dash-point) and the threshold value of timelike region (dotted line): $s = 4m_p^2$.

7 Angular distribution

The experimental apparatus of E-835 doesn't allow to distinguish e^+ and e^-, then to measure the angular distribution we have to consider both angular distribution of the two tracks corresponding at pair e^+e^- . This can be done because the differential cross section of the reaction $\overline{p}p \to e^+e^-$ is symmetric under interchange between e^+e^- .

Since the energies at which form factor events has been found are near, we measure the angular distribution using all these points together in the cm common acceptance. The c.m. common acceptance is defined by smallest value of $|\cos\theta^*|_{max}$ reported in Tab.7, then we choose the interval $-0.55 \leqslant \cos\theta^* \leqslant 0.55$. The angular distribution measured with all energies is reported in Fig.5. It shows also the function $(1+\cos^2\theta^*)$, $(1-\cos^2\theta^*)$ and a constant which are all equally compatible: $\chi^2/ndf = 0.8$, 1.1 and 0.9 respectively.

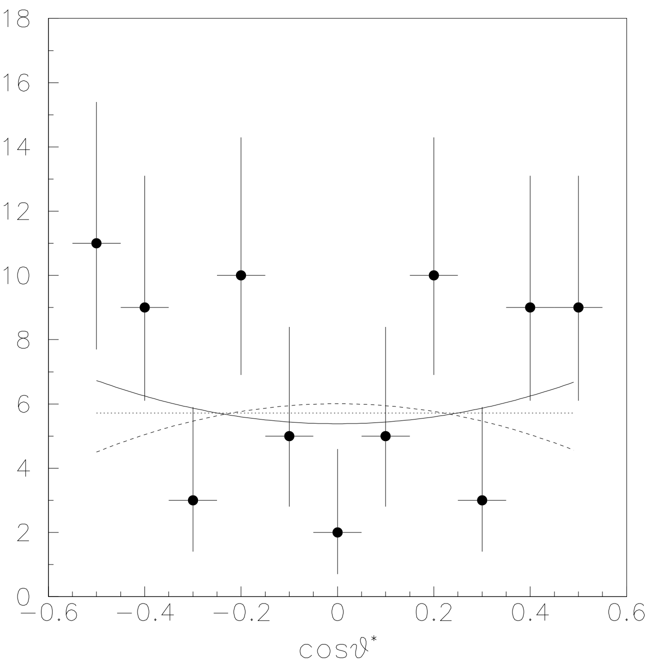

Figure 5: Angular distribution of all form factor events in c.m. common region $-0.55 \leqslant \cos\theta^* \leqslant 0.55$. Two entries for each events. Also shown the function $1+\cos^2\theta^*$ (solid line), $1-\cos^2\theta^*$ (dashed line) and a constant (dotted line).

With the restriction on c.m. common acceptance we lose 4 form factor events at h_c energy, then we try to measure the angular distribution considering only all 31 form factor events at $s = 12.43$ GeV^2 in c.m. common region $-0.60 \leqslant \cos\theta^* \leqslant 0.60$. This angular distribution is reported in Fig.6, in which we also show the function $(1+\cos^2\theta^*)$, $(1-\cos^2\theta^*)$ and a constant which are all equally compatible: $\chi^2/ndf = 0.5$, 0.9 and 0.7 respectively.

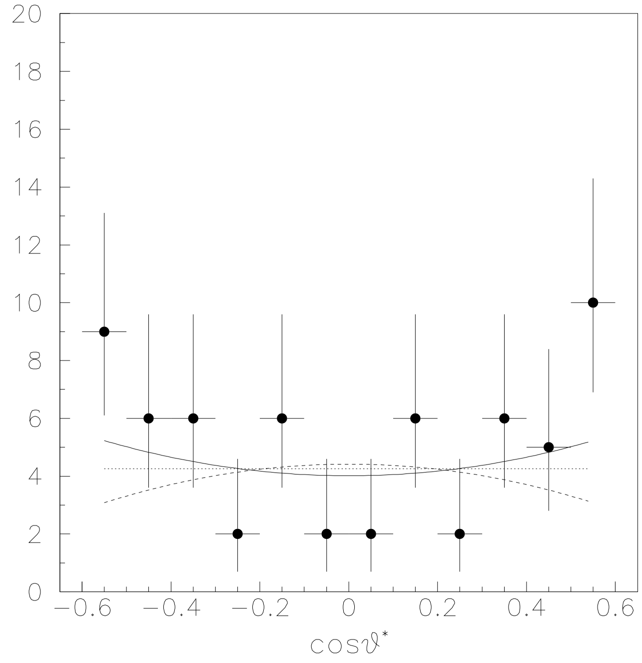

Figure 6: Angular distribution of all 31 form factor events at $s = 12.43$ GeV^2 in c.m. common region $-0.60 \leqslant \cos\theta^* \leqslant 0.60$. Two entries for each events. Also shown the function $1 + \cos^2\theta^*$ (solid line), $1 - \cos^2\theta^*$ (dashed line) and a constant (dotted line).

Since the statistic is low we cannot conclude nothing about the behavior of the angular distribution, but it seems to prefer the $(1 + \cos^2\theta^*)$ behavior as it should be at high energies.

Appendix A

Determination of the analysis efficiency with Monte Carlo simulation

To find the characteristic of the events with e^+e^- in the final state and to test the rejection factor of the form factor selection we use also the simulation of some reactions. Also we use Monte Carlo simulation to calculate the efficiency of charged trigger, preselection and final selection. The results obtained with this efficiency will be compared with the results calculated with efficiency determined by real data. All simulated reaction are reported in Tab.9.

ID	Reaction	E_{cm} (MeV)	RUN
1	$\overline{p}p \longrightarrow e^+e^-$	3526.2	7054
2	"	3418.0	5444
3	"	3510.5	5126
4	"	3555.7	5109
5	"	3800.0	7107
6	$\overline{p}p \rightarrow \chi_0 \rightarrow J/\psi\ \gamma \rightarrow e^+e^-\ \gamma$	3418.0	5444
7	$\overline{p}p \rightarrow \chi_1 \rightarrow J/\psi\ \gamma \rightarrow e^+e^-\ \gamma$	3510.5	5126
8	$\overline{p}p \rightarrow \chi_2 \rightarrow J/\psi\ \gamma \rightarrow e^+e^-\ \gamma$	3555.7	5109
9	$\overline{p}p \rightarrow h_c \rightarrow J/\psi\ \pi^0 \rightarrow e^+e^-\ \pi^0$	3526.2	7054
10	$\overline{p}p \longrightarrow \pi^0\pi^0$	3526.2	5610
11	$\overline{p}p \longrightarrow \pi^0\gamma$	3526.2	7005
12	$\overline{p}p \longrightarrow \gamma\gamma$	3526.2	5753
13	$\overline{p}p \rightarrow \psi' \rightarrow e^+e^-$	3686.0	5572
14	$\overline{p}p \rightarrow \psi' \rightarrow J/\psi\ \pi^0 \rightarrow e^+e^-\ \pi^0$	"	"
15	$\overline{p}p \rightarrow \psi' \rightarrow J/\psi\ \pi^0\pi^0 \rightarrow e^+e^-\ \pi^0\pi^0$	"	"
16	$\overline{p}p \rightarrow \psi' \rightarrow J/\psi\ \pi^+\pi^- \rightarrow e^+e^-\ \pi^+\pi^-$	"	"
17	$\overline{p}p \rightarrow \psi' \rightarrow \chi_0\gamma \rightarrow J/\psi\ \gamma\gamma \rightarrow e^+e^-\ \gamma\gamma$	"	"
18	$\overline{p}p \rightarrow \psi' \rightarrow \chi_1\gamma \rightarrow J/\psi\ \gamma\gamma \rightarrow e^+e^-\ \gamma\gamma$	"	"
19	$\overline{p}p \rightarrow \psi' \rightarrow \chi_2\gamma \rightarrow J/\psi\ \gamma\gamma \rightarrow e^+e^-\ \gamma\gamma$	"	"
20	$\overline{p}p \rightarrow \psi' \rightarrow K^+K^-$	"	"
21	$\overline{p}p \rightarrow \psi' \rightarrow \pi^+\pi^-$	"	"
22	$\overline{p}p \rightarrow \psi' \rightarrow \pi^+\pi^-\pi^0$	"	"
23	$\overline{p}p \rightarrow \psi' \rightarrow 2(\pi^+\pi^-)$	"	"
24	$\overline{p}p \rightarrow \psi' \rightarrow 2(\pi^+\pi^-)\pi^0$	"	"

Table 9: Simulated reaction with Monte Carlo. ID: number of identification; E_{cm}: energy in cm; RUN: referred to the conditions of the detector.

In Tab.10 we report the events which satisfy charged trigger and preselection, also we calculate their efficiencies using only those reactions with an e^+e^- pair in the final state.

ID	N_{gen}	N_{acc}	N_{trigg}	$\epsilon_{trigg}(\%)$	N_{ewdst}	$\epsilon_{ewdst}(\%)$	$\epsilon_{presel}(\%)$
1	10^4	6620±47	5975±24	90±1	5508±21	92.2±0.7	83.2±0.6
2	10^4	6426±48	5808±24	90±1	5373±20	92.5±0.7	83.6±0.7
3	10^4	6614±47	5973±24	90±1	5491±21	91.9±0.7	83±1
4	10^4	6564±47	5955±24	91±1	5471±21	91.9±0.7	83.3±0.7
5	10^4	6097±49	5535±23	91±1	5060±21	91.4±0.7	83.0±0.7
6	10^4	6202±49	5586±24	90±1	5136±20	91.9±0.8	82.8±0.7
7	10^4	6141±49	5481±24	89±1	5043±20	92.0±0.8	82.1±0.7
8	10^4	6116±49	5431±25	89±1	4961±21	91.3±0.8	81.1±0.7
9	10^4	6151±49	5483±24	89±1	5046±20	92.0±0.8	82.0±0.7
10	10^4	6614±47	26±5	×	0^{+2}_{-0}	×	×
11	10^4	6619±47	15±4	×	2±1	×	×
12	10^4	6620±47	0^{+2}_{-0}	×	0^{+2}_{-0}	×	×
13	10^4	6272±48	5665±23	90±1	5206±21	91.9±0.7	83.0±0.7
14	$5\ 10^3$	2981±35	2649±17	89±2	2446±14	92 ±1	82±1
15	$5\ 10^3$	3041±35	2726±17	90±2	2497±14	92 ±1	82±1
16	$5\ 10^3$	3041±35	2617±19	90±2	2441±13	93 ±1	80±1
17	$5\ 10^3$	3005±35	2683±17	90±2	2434±15	91 ±1	81±1
18	$5\ 10^3$	2988±35	2673±17	89±2	2450±14	92 ±1	82±1
19	$5\ 10^3$	2968±35	2620±18	88±2	2387±15	91 ±1	80±1
20	$5\ 10^3$	3093±34	21±5	×	0^{+2}_{-0}	×	×
21	$5\ 10^3$	3145±34	532±21	×	0^{+2}_{-0}	×	×
22	$5\ 10^3$	3002±35	276±16	×	0^{+2}_{-0}	×	×
23	$5\ 10^3$	2381±35	2±1	×	0^{+2}_{-0}	×	×
24	$5\ 10^3$	2373±35	26±5	×	0^{+2}_{-0}	×	×

Table 10: Action of charged trigger and preselection on simulated events. N_{gen}: generated events; N_{acc}: events into fiducial volume; N_{trigg}: events which satisfy the charged trigger; N_{ewdst}: events which satisfy the preselection; $\epsilon_{trigg} = \frac{N_{trigg}}{N_{acc}}$: efficiency of the trigger; $\epsilon_{ewdst} = \frac{N_{ewdst}}{N_{trigg}}$: efficiency of the preselection; $\epsilon_{presel} = \frac{N_{ewdst}}{N_{acc}}$: overall efficiency of trigger and preselection. The efficiencies are calculated only for the reactions with an e^+e^- pair in the final state.

From the charged trigger efficiency of the Tab.10 we find following value for average trigger efficiency:

$$\epsilon^{mc}_{trig} = 0.897 \pm 0.014 \tag{26}$$

Since with real data we calculate the efficiencies of preselection and final selection at ψ' energy, also from Monte Carlo data we want to calculate these efficiencies at same energy, then we simulate the reaction $\psi' \to e^+e^-$ for four different run conditions as reported in Tab.11.

Sample	run	ϵ_{pres}	ϵ_{sel}
1	7277	0.927 ± 0.007	0.642 ± 0.010
2	7144	0.919 ± 0.007	0.653 ± 0.010
3	5078	0.921 ± 0.007	0.645 ± 0.010
4	5572	0.919 ± 0.007	0.641 ± 0.010

Table 11: Simulation of reaction $\psi' \to e^+e^-$ for four different run conditions. ϵ_{pres}: efficiency of the preselection; ϵ_{sel}: efficiency of the final selection.

Averaging the values of ϵ_{pres} in Tab.11 we obtain the following efficiency for the preselection:

$$\epsilon^{mc}_{pres} = 0.921 \pm 0.004(stat)^{+0.013}_{-0.010}(syst) \tag{27}$$

while for the efficiency of the final selection we obtain the value:

$$\epsilon^{mc}_{sel} = 0.645 \pm 0.005(stat)^{+0.018}_{-0.014}(syst) \tag{28}$$

Using the trigger efficiency (26) and the above values we obtain the efficiency of the form factor analysis:

$$\epsilon^{mc}_{ana} = 0.533 \pm 0.010(stat)^{+0.017}_{-0.013}(syst) \tag{29}$$

In Tab.12 we compare the values of form factors calculated with the efficiency estimated by Monte Carlo with the results obtained using the real data.

We can conclude that there is a good agreement between the results obtained with the two efficiency calculated with real and simulated data.

s (GeV^2)	L (pb^{-1})	N	σ_{acc} (pb)	$\|\cos\theta^*\|_{max}$	$10^2 \times \|G_M\|$ (a)	(b)
11.42±0.09	8.52	8	$1.64^{+0.81+0.11}_{-0.57-0.10}$ ($1.76^{+0.87+0.87}_{-0.61-0.61}$)	0.568	$1.74^{+0.43+0.06}_{-0.30-0.05}$ ($1.81^{+0.45+0.45}_{-0.31-0.31}$)	$1.95^{+0.48+0.07}_{-0.34-0.05}$ ($2.02^{+0.50+0.50}_{-0.35-0.35}$)
11.93±0.13	3.95	3	$1.33^{+1.29+0.09}_{-0.72-0.08}$ ($1.42^{+1.39+1.39}_{-0.78-0.78}$)	0.585	$1.59^{+0.77+0.06}_{-0.43-0.05}$ ($1.65^{+0.80+0.80}_{-0.45-0.45}$)	$1.77^{+0.86+0.06}_{-0.48-0.06}$ ($1.83^{+0.89+0.89}_{-0.50-0.50}$)
12.43±0.01	50.50	31	$1.07^{+0.23+0.07}_{-0.20-0.07}$ ($1.15^{+0.25+0.25}_{-0.21-0.21}$)	0.601	$1.45^{+0.15+0.05}_{-0.13-0.04}$ ($1.50^{+0.16+0.16}_{-0.14-0.14}$)	$1.60^{+0.17+0.06}_{-0.15-0.05}$ ($1.66^{+0.18+0.18}_{-0.15-0.15}$)
14.40±0.19	5.17	0	< 0.85 (< 0.90)	0.603	< 1.42 (< 1.47)	< 1.56 (< 1.60)
18.22±0.01	2.10	0	< 2.10 (< 2.22)	0.512	< 2.85 (< 2.94)	< 3.08 (< 3.17)

Table 12: Summary of the results of the form factor analysis using real efficiency. The results obtained with Monte Carlo efficiency are shown between parenthesis. $\sigma_{acc} = N/(\epsilon \cdot L)$; $|\cos\theta^*|_{max}$ is the maximum value of $|\cos\theta^*|$ where θ^* is the scattering angle in c.m.; (a) $|G_M|$ calculated in the hypothesis $|G_E| = |G_M|$; (b) $|G_M|$ calculated in the approximation of negligible electric contribution. Between parenthesis we report the results obtained with MC efficiency.

Appendix B

Efficiency of the form factor analysis using real sample of data

In Appendix A we have calculated the efficiency of the form factor analysis using Monte Carlo simulation. Here we will calculate the efficiency using real data at ψ' energy, selecting a clean sample of $\psi' \to e^+e^-$ events.

Efficiency of charged trigger

The efficiency of charged trigger has been calculated with some special trigger runs (5818-5837) at formation energy of ψ' collecting an integrated luminosity of 0.99 nb^{-1}. It is:

$$\epsilon_{trig}^{data} = 0.90 \pm 0.02 \tag{30}$$

Efficiency of off-line preselection

The efficiency of preselection has been calculated using four samples of mdst data as reported in Tab.13 [7].

sample	run	E_{cm}	$\int Ldt$ (pb^{-1})
1	5006-5038 5076-5084 5076-5084 5076-5084	ψ' peak	2.40
2	5571-5574 5818-5837 5840-5842 7143-7148	ψ' peak	4.95
3	7248-7252 7254-7259 7269-7271	ψ' peak + bckg	4.52
4	7273-7278	ψ' peak	1.94

Table 13: Samples of mdst data used in the calculation of preselection efficiency.

We have extracted clean samples of $\psi' \to e^+e^-$ events requiring only two cluster on-time (corresponding to the e^+e^- pair) and applying tight topological cuts relative to two body hypothesis. Then applying the preselection we find the efficiency reported in Tab.14

[7] Stacks 5 and 6 have not been used, because there are no events with ψ' invariant mass.

sample	ϵ_{pres}
1	0.969 ± 0.021
2	0.960 ± 0.030
3	0.966 ± 0.024
4	0.967 ± 0.026

Table 14: Efficiency of the preselection obtained from real sample of $\psi' \to e^+e^-$ events.

Averaging the values of Tab.14 we obtain the following preselection efficiency:

$$\epsilon_{pres}^{data} = 0.966 \pm 0.013(stat)^{+0.027}_{-0.036}(syst) \tag{31}$$

Efficiency of final selection and of form factor analysis

We have calculated the efficiency of the final selection using four sample of preselected data at formation energy of ψ' and subtracting the background above and below ψ' peak and J/ψ inclusive events at ψ' peak with $M_{ee} > 3.4$ GeV. Four samples and two background are reported in Tab.15 [8].

Sample	run	E_{CM} (MeV)	$\int Ldt$ (pb^{-1})
1	$5006 \div 5084$	3686	1.756
2	$5571 \div 5574$		
	$5818 \div 5842$	3686	2.380
3	$7144 \div 7259$	3686	5.944
4	$7273 \div 7278$	3686	2.401
bkg	$7280 \div 7283$	3666	0.779
bkg	$7269 \div 7271$	3704	1.153

Table 15: Four samples at the ψ' peak and two background above and below the peak.

The restriction on fiducial volume will be taken into account in the integration of differential cross section. Then to evaluate the efficiency of final selection we have to consider the three cuts:

$$[Prb(e^+e^-) > Prb(J/\psi + X)] \text{ and } [Prb(e^+e^-) > 1\%] \tag{32}$$

$$\log_{10}(ew1 * ew2) > 0 \tag{33}$$

$\forall$ *extra cluster ontime*

$$[M_{\gamma e_1} \leqslant 100 \text{ MeV}] \text{ or } [M_{\gamma e_2} \leqslant 100 \text{ MeV}] \tag{34}$$

[8] Stacks 5 and 6 are not been used, because there are not events with ψ' invariant mass.

Subtracting the background at two different energies we obtain the eight values of the final selection efficiency reported in Tab.16.

Sample	ϵ_{sel}
1	$0.716^{+0.030}_{-0.029}$
2	$0.654^{+0.029}_{-0.028}$
3	$0.666^{+0.019}_{-0.017}$
4	$0.682^{+0.025}_{-0.024}$

(a)

Sample	ϵ_{sel}
1	$0.716^{+0.030}_{-0.029}$
2	$0.653^{+0.029}_{-0.028}$
3	$0.665^{+0.018}_{-0.017}$
4	$0.682^{+0.025}_{-0.024}$

(b)

Table 16: Efficiency of final selection: (a) background at 3666 MeV, (b) background at 3704 MeV

Averaging the values in Tab.16 the final selection efficiency results:

$$\epsilon_{sel}^{data} = 0.679 \pm 0.009(stat)^{+0.037}_{-0.026}(syst) \tag{35}$$

The efficiency of the form factor analysis is $\epsilon_{ana}^{data} = \epsilon_{trig}^{data} \cdot \epsilon_{pres}^{data} \cdot \epsilon_{sel}^{data}$:

$$\epsilon_{ana}^{data} = 0.590 \pm 0.017(stat)^{+0.036}_{-0.032}(syst) \tag{36}$$

Alternative calculation of the analysis efficiency

To find the efficiency of final selection using a different method we have to calculate separately the efficiency of each single cut (32), (33) and (34), because we select a clean sample of $\psi' \to e^+e^-$ events using tight cuts, as described below.

Efficiency of the cut (32) has calculated extracting a clean sample of e^+e^- final states obtained requiring:

$$M_{ee} > 3.4 \text{ GeV} \tag{37}$$

$$\log_{10}(ew1 * ew2) > 1 \tag{38}$$

$$\text{cut (34)} \tag{39}$$

Efficiency of the cut (33) has been calculated extracting a clean sample of e^+e^- final states obtained requiring:

$$M_{ee} > 3.4 \text{ GeV} \tag{40}$$

$$Prb(e^+e^-) > Prb(J/\psi X) \text{ and } Prb(e^+e^-) > 10\% \tag{41}$$

$$\text{cut (34)} \tag{42}$$

Efficiency of the cut (34) has been calculated extracting a clean sample of e^+e^- final states obtained requiring:

$$M_{ee} > 3.4 \text{ GeV} \tag{43}$$

$$Prb(e^+e^-) > Prb(J/\psi X) \text{ and } Prb(e^+e^-) > 1\% \tag{44}$$

$$\log_{10}(ew1 * ew2) > 0 \tag{45}$$

Subtracting the background at two different energies we obtain the eight values of the final selection efficiency reported in Tab.17.

Sample	ϵ_{sel}
1	$0.724^{+0.038}_{-0.035}$
2	$0.675^{+0.039}_{-0.034}$
3	$0.682^{+0.027}_{-0.021}$
4	$0.697^{+0.032}_{-0.030}$

(a)

Sample	ϵ_{sel}
1	$0.723^{+0.037}_{-0.035}$
2	$0.675^{+0.038}_{-0.035}$
3	$0.681^{+0.025}_{-0.022}$
4	$0.697^{+0.032}_{-0.030}$

(b)

Table 17: Efficiency of final selection: (a) background at 3666 MeV, (b) background at 3704 MeV

Averaging the values in Tab.17 the final selection efficiency results:

$$\epsilon_{sel}^{dataII} = 0.694^{+0.012}_{-0.011}(stat)^{+0.030}_{-0.020}(syst) \tag{46}$$

The efficiency of form factor analysis is $\epsilon_{ana}^{data} = \epsilon_{trig}^{data} \cdot \epsilon_{pres}^{data} \cdot \epsilon_{sel}^{data}$ and results:

$$\epsilon_{ana}^{dataII} = 0.604^{+0.019}_{-0.018}(stat)^{+0.031}_{-0.028}(syst) \tag{47}$$

perfectly consistent to the efficiency calculated with the other method.

Appendix C

Stability of the Selection Criteria

The cuts for event selection are stable in proximity of the values used in the final selection. This result come from the behavior of th ratio N/ϵ as a function of different values used in the cuts of event selection. In Fig.7 we report the efficiency of event selection as a function of each cut. These efficiencies are been calculated with real data at ψ' energy.

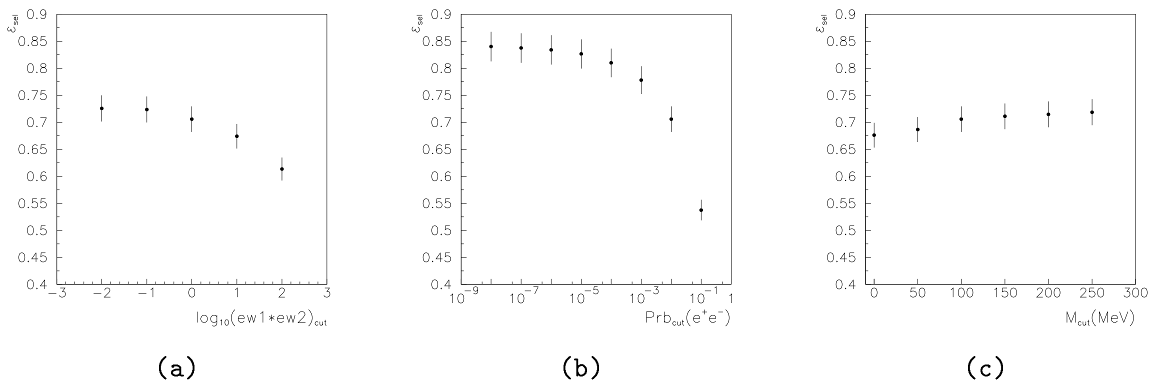

Figure 7: Efficiency of the off-line selection as a function of each cut. (a): fixing the cuts (4) and (6). (b): fixing the cuts (5) and (6). (c): fixing the cuts (4) and (5).

In following Figures we show the number of form factor events and the ratio N/ϵ as a function of each cut at the three different energies used.

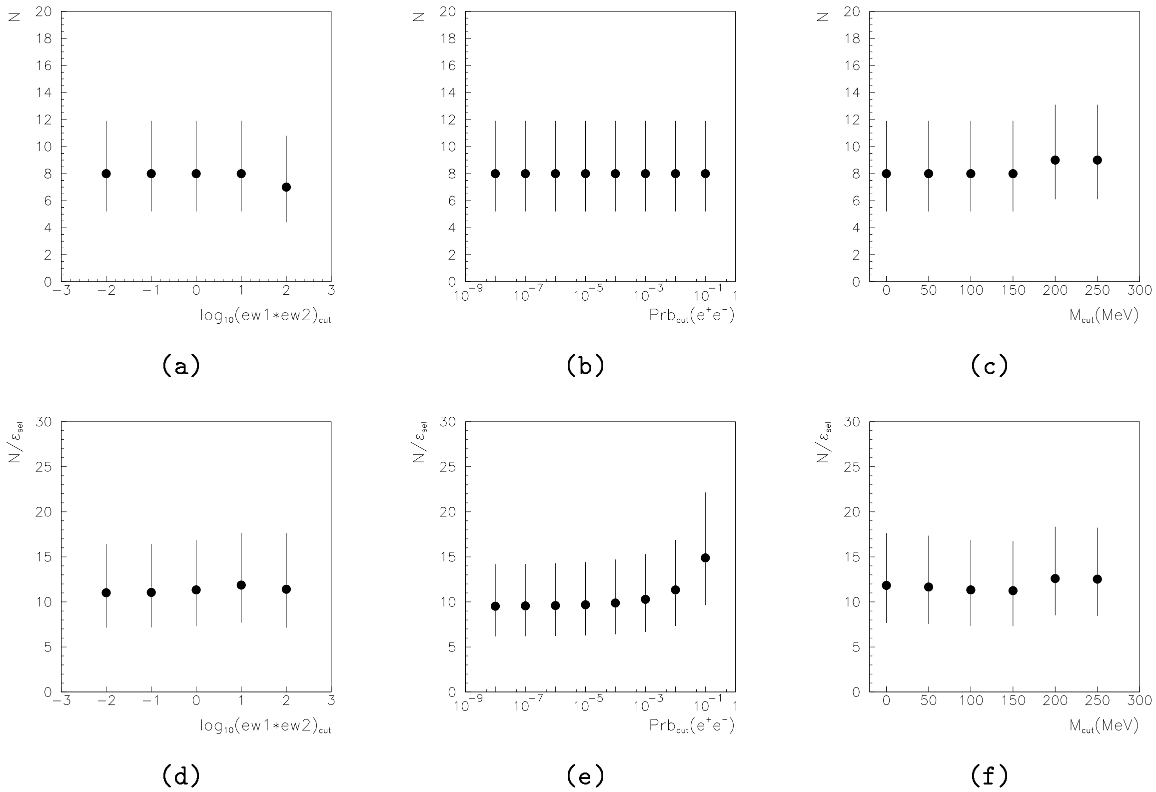

Figure 8: Number of events N selected at $s = 11.42$ GeV^2 and ratio N/ϵ as a function of each cut. `(a)(d)`: fixing the cuts (4) and (6). `(b)(e)`: fixing the cuts (5) and (6). `(c)(f)`: fixing the cuts (4) and (5).

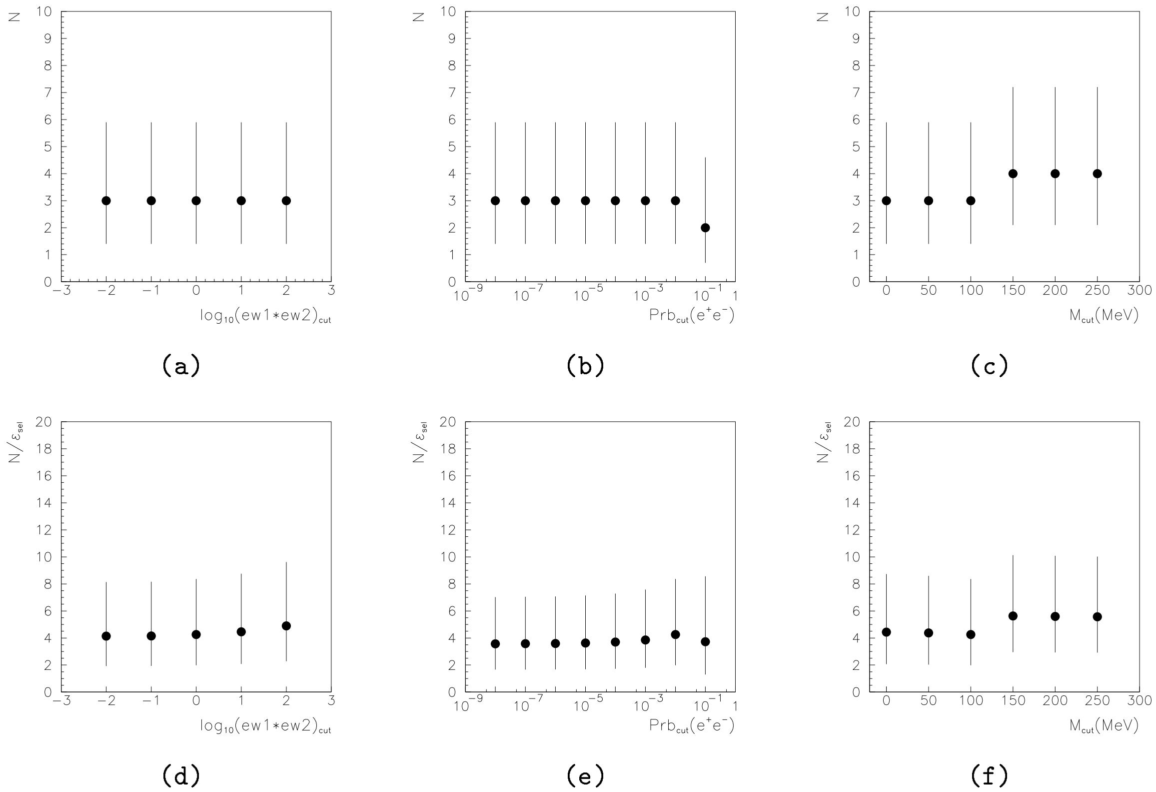

Figure 9: Number of events N selected at $s = 11.93$ GeV^2 and ratio N/ϵ as a function of each cut. `(a)(d)`: fixing the cuts (4) and (6). `(b)(e)`: fixing the cuts (5) and (6). `(c)(f)`: fixing the cuts (4) and (5).

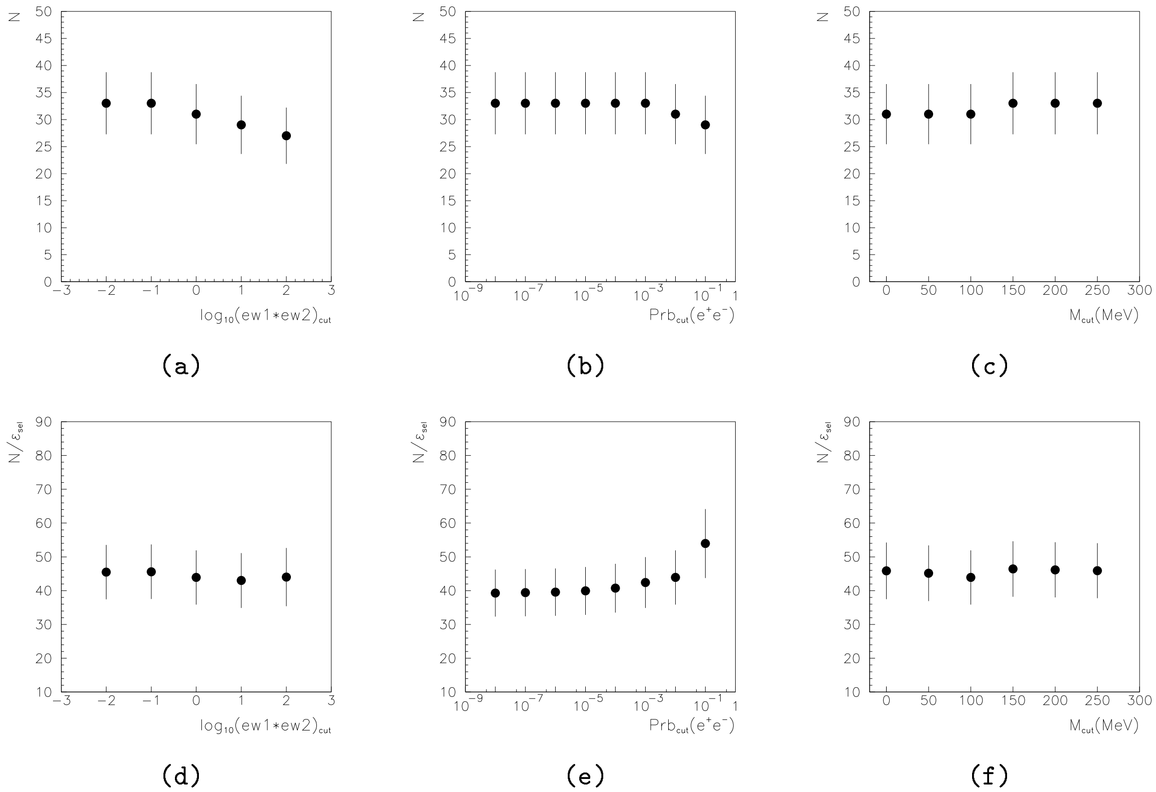

Figure 10: Number of events N selected at $s = 12.43$ GeV^2 and ratio N/ϵ as a function of each cut. `(a)(d)`: fixing the cuts (4) and (6). `(b)(e)`: fixing the cuts (5) and (6). `(c)(f)`: fixing the cuts (4) and (5).

Appendix D

Photon conversions

Selection of $\pi^0\pi^0$ events

To estimate the contribution from background reaction (13), (14) and (15) we have to know the probability η that a photon convert into an e^+e^- pair before hodoscope H1.
To measure this probability we have used data from a special total-energy trigger without hodoscopes in veto. This trigger requires that the energy deposited in CCAL be at least 80% of the total energy in laboratory frame (ETOT 80% no-veto).
From this data a sample of $\pi^0\pi^0 \to 4\gamma$ has been selected requiring exactly 4 clusters in CCAL. To identify the two photons coming from the same pion we make all possible combinations of two pairs of cluster and we choose that which minimizes the variable:

$$f = \sqrt{(\Delta\theta)^2 + (\Delta\phi)^2} \tag{48}$$

where:
$\Delta\phi = \left|\phi_{\pi^0_1} - \phi_{\pi^0_2}\right| - \pi$
$\Delta\theta = \theta_{\pi^0_1 p} - \theta_{\pi^0_1 m}$
$\theta_{\pi^0_1 m}$ is the polar angle of the forward pion calculated from the directions and energies of the two photons, $\theta_{\pi^0_1 p}$ is the same angle calculated with kinematics relation relative to $\pi^0\pi^0$ hypothesis using $\theta_{\pi^0_2 m}$ of the backward pion.
In figure Fig.11 are reported the distribution of $\Delta\theta$, $\Delta\phi$ and $M_{\gamma\gamma}$ for candidate $\pi^0\pi^0$ events which minimize the variable f.

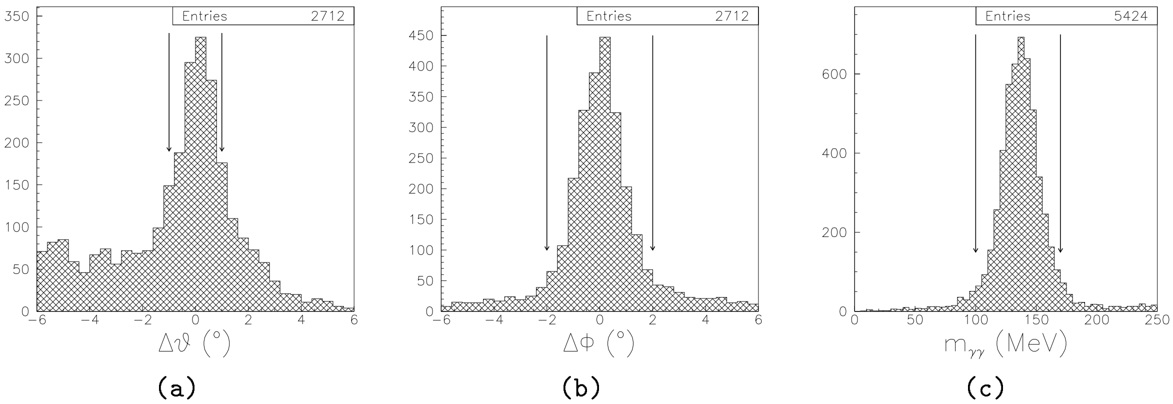

Figure 11: (a) (b) (c) are respectively the distribution of $\Delta\theta$, $\Delta\phi$, $M_{\gamma\gamma}$ for candidate $\pi^0\pi^0$ events. All distributions are obtained requiring $|\Delta\theta| \leq 6^o$ and $|\Delta\phi| \leq 6^o$. On the plots the limits, used to select clean sample of $\pi^0\pi^0$ events, are also reported.

From above distribution we select a clean sample of $\pi^0\pi^0$ events requiring the following restrictions:

$$|\Delta\phi| \leq 1^o \tag{49}$$

$$|\Delta\theta_{cm}| \leq 2^o \tag{50}$$

$$|M_{\gamma\gamma} - m_{\pi^0}| \leq 35 \text{ MeV} \tag{51}$$

we obtain a sample of 1055 events, or 4220 tracks.

Measurement of the probability η

To calculate η we have to take into account that pion undergoes Dalitz decay with a probability $\delta = 1.2\%$, then η results:

$$\eta = \frac{P}{4} - \frac{\delta}{2} \tag{52}$$

where $P = \frac{N(\pi^0\pi^0 \to (e^+e^-)3\gamma)}{N_{tot}(\pi^0\pi^0)}$ is the fraction of events with only one charged track. A charged track is defined as the coincidence between two hodoscopes: H1 and H2 or H1 and HP and requiring a signal above a certain threshold:

$$(ADC_{H1} > 0.5 \text{ mip}) \text{ and } (ADC_{H2} > 1.0 \text{ mip})$$
$$\text{or}$$
$$(ADC_{H1} > 0.5 \text{ mip}) \text{ and } (ADC_{HP} > 1.0 \text{ mip})$$

Since the opening angle of the photons coming from the same pion is small compared to the hodoscope granularity, often if one of the two photons is associable with an hodoscope line, the other one is too. Then, assuming that $\eta^2, \eta \cdot \delta \ll \eta$, each time both photons are recognized as two charged tracks we consider as a single conversion or a Dalitz decay. From the relation (52) we obtain $\eta = 0.9\%$, while from the Fig.12, which show $\eta + \frac{\delta}{2}$ as a function of θ and ϕ, we obtain the maximum value $\eta = 1.7\%$. In the estimation of background cross section we have used this last value.

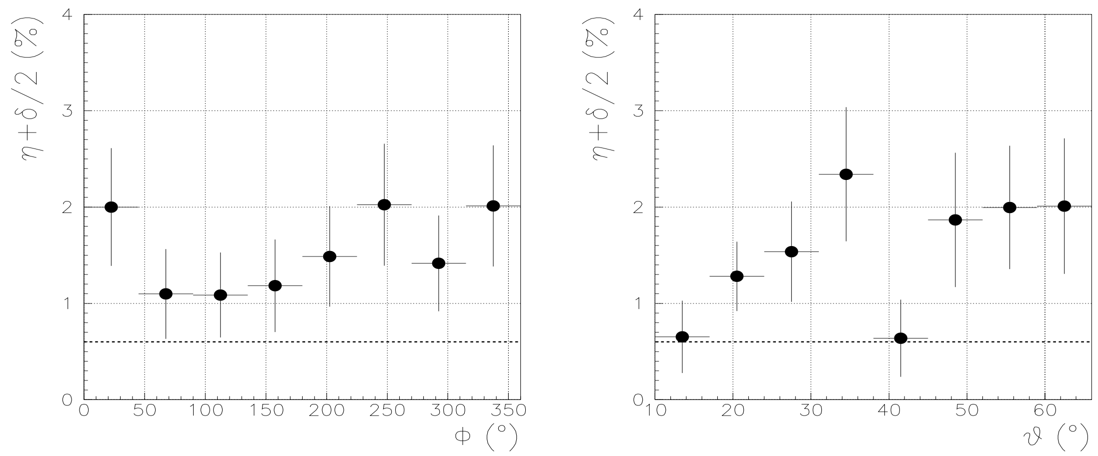

Figure 12: $\eta + \frac{\delta}{2}$ as a function of ϕ and θ obtained from $\pi^0\pi^0$ sample. Dashed lines indicate the value of $\frac{\delta}{2}$.

Measure of the probability ω

Using the same data used to extract $\pi^0\pi^0$ events we select events with two charged tracks requiring at least the presence of a π^0, defined pairing one of the two charged tracks with another cluster. The presence of a π^0 ensure us that the two charged tracks are two pairs e^+e^- , probably coming from a photon conversion or from a Dalitz decay. The fraction of these events which satisfy the cut $\log_{10}(ew1 * ew2) > 0$ used in the form factor analysis is $\omega \approx 10^{-2}$. The distribution of $\log_{10}(ew1 * ew2)$ for a sample of pairs is reported in Fig.13

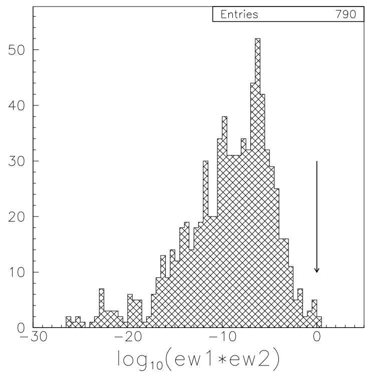

Figure 13: Distribution of EW index for a sample of events with two pairs e^+e^- .

Cross section for the reaction $\overline{p}p \to \pi^0\pi^0$

In Fig.14 we report the cross section for the reaction $\overline{p}p \to \gamma\gamma$ and the cross section for $\pi^0\pi^0$ and $\pi^0\gamma$ final state simulating $\gamma\gamma$ based upon E-760 data and Monte Carlo calculation [8].

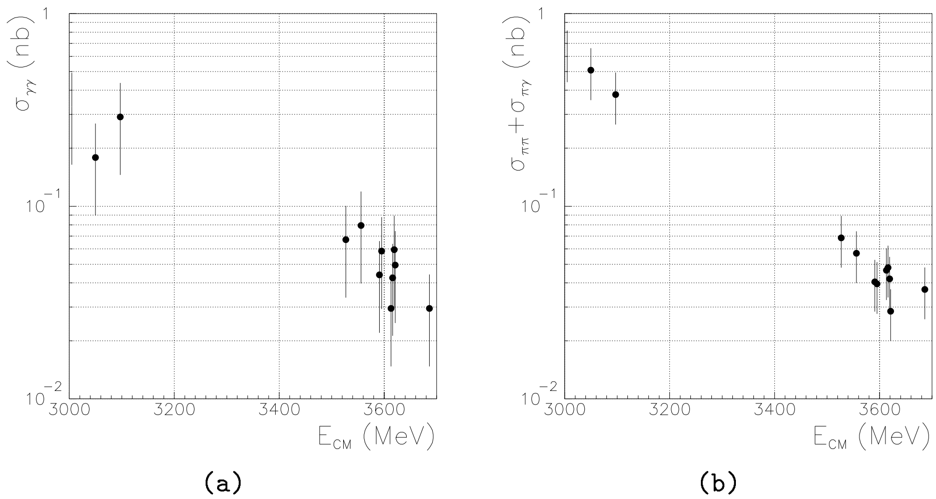

Figure 14: Cross section for $\gamma\gamma$ final state (a) and cross section for $\pi^0\pi^0$ and $\pi^0\gamma$ final state simulating $\gamma\gamma$ (b) integrated over E835 fiducial volume.

The values of these cross section have been used to calculate the expected background cross section from the reaction (13)(14)(15).

Appendix E

Pion rejection

Selection of $\pi^+\pi^-$ events

To estimate the background contamination from the reaction $\overline{p}p \to \pi^+\pi^-$ we have selected a clean sample of these events using data from two-body hadronic trigger, which is used to measure the efficiency of $\overline{p}p$ trigger. The logic of the two-body hadronic trigger is:

$$(\overline{p}p \text{ control}) = (2h) \times (H2 = 2) \times (COPL) \times (\overline{FCH}) \times (SF = 2) \tag{53}$$

We have first preselected the data eliminating the events with $\overline{p}p$ kinematics.
In Fig.15 we report the distribution of $(|\phi_1 - \phi_2| - \pi)$ and of $(\cos\theta_1^* + \cos\theta_2^*)$, where θ^* is the polar angle in CM frame calculated under the assumption that the particle is a pion.

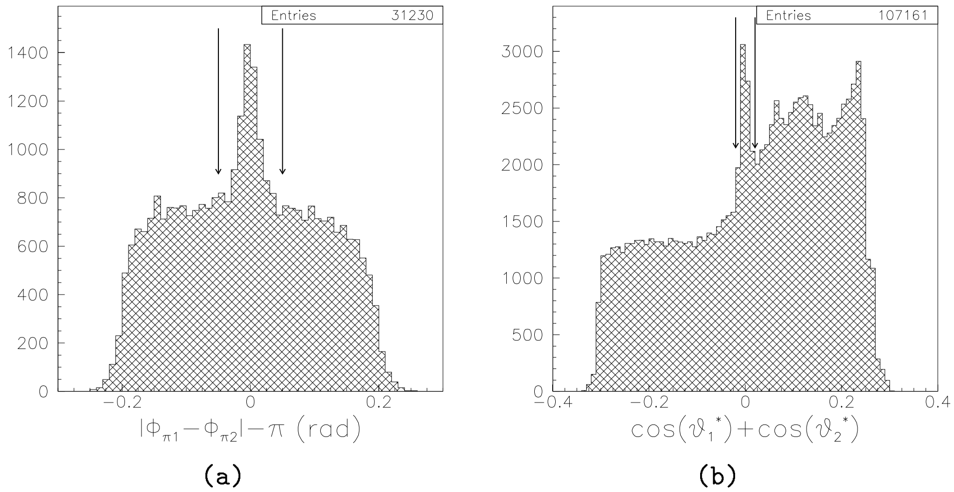

Figure 15: (a) (b) are respectively the distribution of $(|\phi_1 - \phi_2| - \pi)$ and of $(\cos\theta_1^* + \cos\theta_2^*)$ for preselected events. Distribution (a) has been obtained applying the cut (64), while distribution (b) has been obtained applying the cut (63).

To select $\pi^+\pi^-$ events we require:

$$||\phi_1 - \phi_2| - \pi| < 0.05 \text{ rad} \tag{54}$$

$$|\cos\theta_1^* + \cos\theta_2^*| < 0.02 \tag{55}$$

Evaluation of background contamination from $\pi^+\pi^-$

A way to estimate the background contamination is to measure the fraction ϵ of $\pi^+\pi^-$ events which satisfy the form factor analysis, then the expected background cross section can be calculated from the relation (56):

$$\sigma_h = \epsilon \cdot (\alpha_{acc}\sigma_{\pi^+\pi^-}) \tag{56}$$

Since in our sample (9890 events) of $\pi^+\pi^-$ no events satisfy the form factor analysis, we can only derive an upper limit, which is comparable with the value of the cross section for the reaction $\overline{p}p \to e^+e^-$. In order to improve improve this estimate we used two different methods, which are described below.

Method I. Evaluation of background with EW and CCAL rejection powers

To select form factor events we have used two independent cuts: the cut on the EW (57) and the cut on the kinematic (58):

$$\log_{10}(ew1 * ew2) > 0 \tag{57}$$

$$Prb(e^+e^-) > Prb(J/\psi X) \text{ and } Prb(e^+e^-) > 1\% \tag{58}$$

then it is possible to express σ_h in the following form:

$$\sigma_h^{'} = P_{ew} \cdot P_{fit} \cdot (\alpha_{acc}\sigma_{\pi^+\pi^-}) \tag{59}$$

where P_{ew} is the fraction of $\pi^+\pi^-$ events which satisfy the cut (57) and P_{fit} is that fraction which satisfy the cut (58). We obtain that 2 events satisfy the EW cut and zero events satisfy the kinematic cut, that is: $P_{ew} \approx 2 \cdot 10^{-4}$ and $P_{fit} < 2.4 \cdot 10^{-4}$ (upper limit), then $\sigma_h^{'} < 5 \cdot 10^{-2}$ pb. Just this upper limit indicates that background contamination from $\pi^+\pi^-$ is negligible, but we can improve this estimation using another form for σ_h:

$$\sigma_h^{''} = P_{ew} \cdot \xi^2 \cdot (\alpha_{acc}\sigma_{\pi^+\pi^-}) \tag{60}$$

where $\xi \approx 10^{-2}$ is the rejection power of CCAL for single track, that is, the fraction of pions which release a value of energy in CCAL compatible with the value released from an electron with same direction (the measurement of ξ is described below). Then the expected background contamination is:

$$\sigma_h^{''} \approx 2 \cdot 10^{-2}\text{pb} \tag{61}$$

Measurement of ξ

To measure ξ we have to consider the distribution of the variable δE, defined as:

$$\delta E = \frac{|E_p - E_m|}{E_p} \tag{62}$$

where E_m is the energy of the particle measured from CCAL; E_p is the predicted energy of an electron calculated from the value of the polar angle. Integrating the distribution of δE (Fig.16(a)) one obtains the value of ξ as a function of δE of the track (Fig.16(b)).

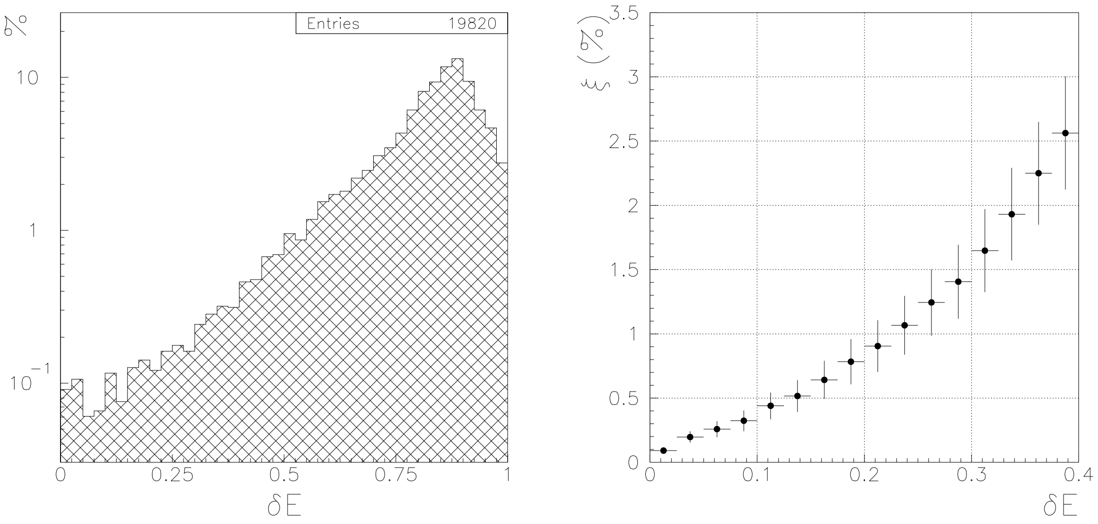

(a) (b)

Figure 16: Distribution of δE (a) and ξ versus δE (b)for the sample of pions.

The value of $\xi \approx 10^{-2}$ has been chosen at $\delta E = 20\%$ (about twice of the resolution of CCAL), because above this value the contribution from electrons is negligible, as shown in the distribution of δE of Fig.17.

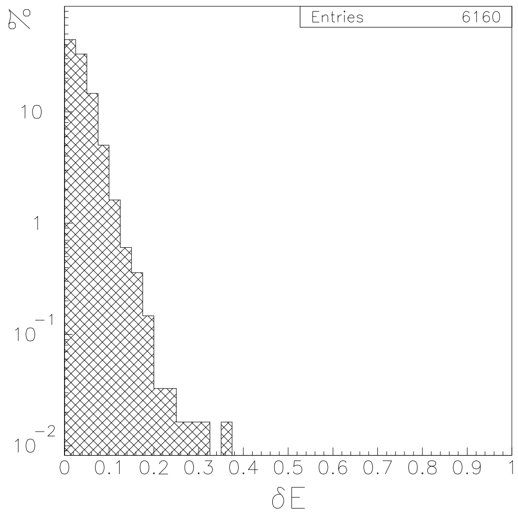

Figure 17: Distribution of δE for a sample of e^+e^- selected with: $Prb(e^+e^-) > Prb(J/\psi X)$, $Prb(e^+e^-) > 1\%$ and $(ew1 * ew2) > 0.1$ at ψ' energy.

Method II. Evaluation of background with Čerenkov and CCAL rejection powers

Instead of using P_{ew} we can consider the following form for σ_h [9]:

$$\sigma_h^{'''} = k^2 \cdot \xi^2 \left(\alpha_{acc}\sigma_{\pi^+\pi^-}\right) \tag{63}$$

where $k \approx 6 \cdot 10^{-3}$ is the rejection power of Čerenkov for single track; in short: k is the probability that a pion release a number of photoelectrons in Čerenkov compatible with the number released from an electron. The method used to measure k is described below. With the relation (63) we find:

$$\sigma_h^{'''} \approx 4 \cdot 10^{-3} \tag{64}$$

which is about $\frac{1}{5}$ of $\sigma_h^{''}$ obtained with method I. This difference is due to the fact that EW is a variable which use not only Čerenkov signal, but informations from hodoscopes and calorimeter. Then if the Čerenkov signal is not compatible with electron hypothesis, but from other detector we have signals compatible with an electron we could have an $(ew1 * ew2)$ similar to the value for an e^+e^- event.

Measurement of k

To measure k we have to study the normalized distribution of Čerenkov signals for electrons (preselected with $ew1 * ew2 > 0.1$) and for pions plotted in Fig.18(a).

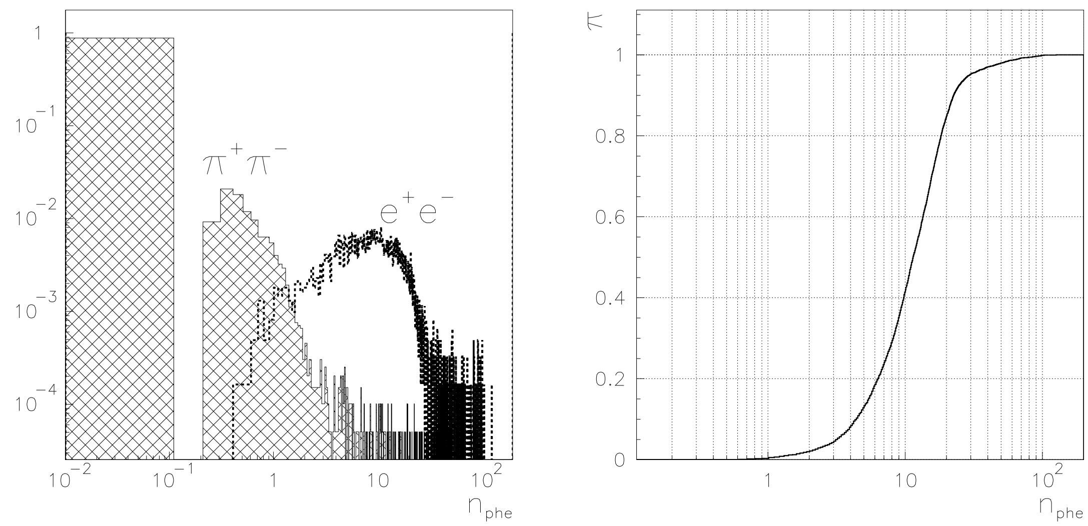

(a) (b)

Figure 18: Distribution of Čerenkov signal for clean sample of electron tracks and for pion tracks (a), probability Π versus n_{phe} (b).

The distribution of Čerenkov signal for electrons is the derivative of the probability Π of passing the cut on the EW $(ew1 * ew2 > 0.1)$. The probability Π is constrained to be zero at $n_{phe} = 0$ and approaches one as n_{phe} increases, as we can see in Fig.18(b) obtained integrating the distribution for electrons in Fig.18(a).

The probability k for a pion track to pass the EW cut due to Čerenkov signal is obtained multiplying this distribution by Π and summing over n_{phe}. The results is $k \approx 6 \cdot 10^{-3}$.

[9] This is the same method used in the runI analysis [3][29].

Cross section for the reaction $\overline{p}p \to \pi^+\pi^-$

In the above discussion we have always used the value $\alpha_{acc}\sigma_{\pi^+\pi^-} \approx 10^6$ pb, which is the order of magnitude of this cross section at our energies. In order to be more accurate in the evaluation of the background contamination we use at different energies the corresponding values of $\alpha_{acc}\sigma_{\pi^+\pi^-}$ extracted from the plot in Fig.19.

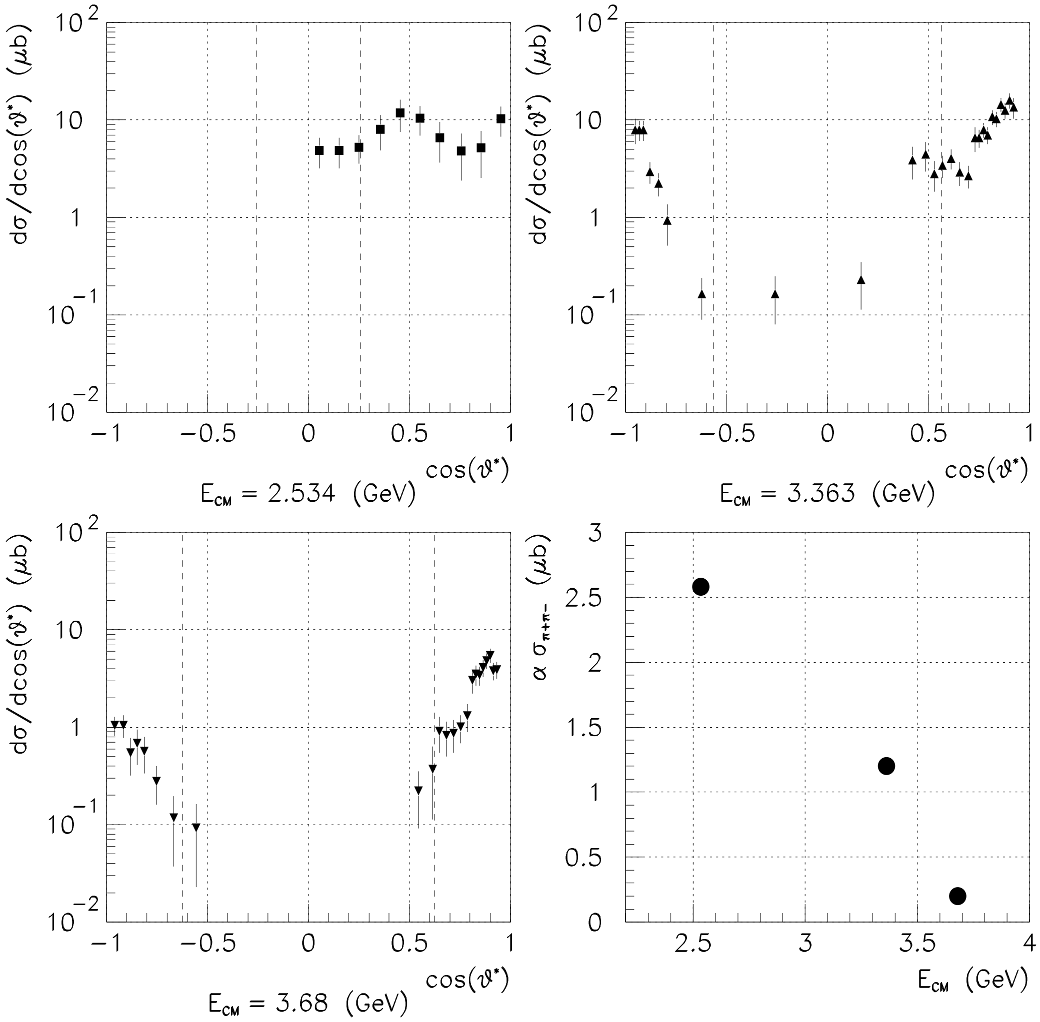

Figure 19: Differential $\overline{p}p \to \pi^+\pi^-$ cross section taken from the literature [5][6][7]. The bottom right plot shows the cross section integrated over E835 fiducial volume(vertical dashed lines in the other three plots), as a function of CM energy.

References

[1] W. Baldini(2001). *The charged trigger efficiency of E835-runII.* Fermilab E-835, Not published.

[2] G. Stancari(1998). *Measurement of the Magnetic Form Factor of the Proton.* FNAL E760/E835 Internal Memo No.369.

[3] G. Stancari(1998). *Measurements of th Magnetic Form Factor of the Proton for Large Time-like Momentum Transfers.* Doctoral Dissertation, Università degli Studi di Ferrara.

[4] T.A. Armstrong et al.(1992). *Observation of the $^1P_1$ State of Charmonium.Phys. Rev. Lett.* **69**(16),2337-2340.

[5] T.Fields et al.(1972). *Comparison of new data on $\overline{p}p \to \pi^+\pi^-$ and other two meson states at 2.3 GeV/c.Phys. Lett.* **40B**(4),503-506.

[6] A.Eide et al.(1973). *Elastic scattering and two-body annihilations at 5 GeV/c.Nucl. Phys.* **B60**,173-220.

[7] T.Buran et al.(1976). *Antiproton-proton annihilation into $\pi^+\pi^-$ an K^+K^- at 6.2 GeV/c.Nucl. Phys.* **B116**,51-64.

[8] T.A. Armstrong et al.(1997). *Two-body neutral final states produced in antiproton-proton annihilations at* $2.911 \le \sqrt{s} \le 3.686$ *GeV.Phys. Rev. D* **56**(5),2509-2531.

[9] M. Ambrogiani et al.(2000). *Study of the $\gamma\gamma$ decays of the $\chi_{c2}\left(1^3P_2\right)$ and $\chi_{c0}\left(1^3P_0\right)$ charmonium resonances.Phys. Rev. D* **62**(5),052002.

[10] R. W. McAllister and R. Hofstadter(1956). *Elastic Scattering of 188-MeV Electrons from the Proton and Alpha Particle. Phys. Rev.* **102**(3),851-856.

[11] M. Conversi et al.(1965). *The Leptonic Annihilation Modes of the Proton-Antiproton System at 6.8$(GeV/c)^2$ Timelike Four-Momentum Transfer. Nuovo Cimento* **XLA**(2),690-701.

[12] D. L. Hartill et al.(1969). *Antiproton-Proton Annihilation into Electron-Positron Pairs and Gamma-Ray Pairs. Phys. Rev.* **184**(5),1415-1423.

[13] M. Castellano et al.(1973). *The Reaction $e^+e^- \to \overline{p}p$ at a Total Energy of 2.1 GeV. Nuovo Cimento* **14A**(1),1-20.

[14] W. Braunschweig et al(1975). *Two Body Hadronic Decays of the 3.1 GeV Resonance. Phys. Lett.* **57B**(3),297-300.

[15] G. Bassompierre et al.(1976). *Measurement of the Branching Ratio $\Gamma(\overline{p}p \to e^+e^-)/\Gamma(\overline{p}p \to$ total) in Antiproton-Proton annihilation at rest. Phys. Lett.* **64B**(4),475-478.

[16] G. Bassompierre et al.(1976). *First Determination of the Proton Electromagnetic Form Factors at the Threshold of the Time-Like Region. Phys. Lett.* **68B**(5),477-479.

[17] B. Delcourt et al.(1979). *Study of the Reaction $e^+e^- \to \overline{p}p$ in the Total Energy Range 1925-2180 MeV. Phys. Lett.* **86B**(3,4),395-398.

[18] D. Bisello et al.(1983). *A Measurement of $e^+e^- \to \overline{p}p$ for (*$1975 \leqslant \sqrt{s} \leqslant 2250$*) MeV. Nucl. Phys. B* **224**,379-395.

[19] D. Bisello et al.(1990). *Barion pairs production in* e^+e^- *annihilation at* $\sqrt{s} = 2.4$ *GeV. Z. Phys. C* **48**,23-28.

[20] C. Baglin et al.(1985). *Upper Limits of the Proton Magnetic Form Factor in the Time-like Region from* $\overline{p}p \to e^+e^-$ *at the CERN-ISR. Phys. Lett.* **163B**(5,6),400-403.

[21] G. Bardin et al.(1991a). *Measurement of the proton electromagnetic form factor near threshold in the time-like region. Phys. Lett. B* **255**(1),149-154.

[22] G. Bardin et al.(1991b). *Precise determination of the electromagnetic form factor in the time-like region up to* $s = 4.2$ GeV^2. *Phys. Lett. B* **257**(3,4),514-518.

[23] G. Bardin et al.(1994). *Determination of the electric and magnetic form factors of the proton in the time-like region. Nucl. Phys. B* **411**,3-32.

[24] A. F. SIll et al.(1993). *Measurements of elastic electron-proton scattering at large momentum transfer. Phys. Rev. D* **48**(1),29-55.

[25] R. C. Walker et al.(1994). *Measurements of the proton elastic form factor for* $1 \leqslant Q^2 \leqslant 3$ $(GeV/c)^2$ *at SLAC. Phys. Rev. D* **49**(11),5671-5689.

[26] A. Antonelli et al.(1994). *Measurement of the electromagnetic form factor of the proton in the time-like region. Phys. Lett.* **69**(16),2337-2340.

[27] L. Andivahis et al.(1994). *Measurements of the electric and magnetic form factor of the proton from* $Q^2 = 1.75$ *to 8.83* $(GeV/c)^2$. *Phys. Rev. D* **60**(9),5491-5517.

[28] T.A. Armstrong et al.(1993). *Proton Electromagnetic Form Factor in Timelike Region from 8.9 to 13.0* GeV^2. *Phys. Rev. Lett.* **70**(9),1212-1215.

[29] M. Ambrogiani et al.(1999). *Measurements of the magnetic form factor of the proton in timelike region at large momentum transfer.Phys. Rev. D* **60**(3),032002(1-6).

[30] C. Caso et al.(1998). *Review of Particle Physics.Euro. Phys. J. C* **3**(1-4),1-794.

[31] D. R. Yennie, M. M. Lévi and D. G. Ravenhall(1957). *Electromagnetic Structure of Nucleons. Phys. Mod. Rev.* **29**(1),144-157.

[32] F. J. Ernst, R. G. Sachs and K. C. Wali(1960). *Electromagnetic Form Factor of the Nucleon. Phys. Rev.* **119**(3),1105-1114.

[33] N. Cabibbo and R. Gatto(1961). *Electron-Positron Colliding Beam Experiments.Phys. Rev.* **124**(5),1577.

[34] M. Jacob, G. C. Wick(1959). *On the General Theory of Collisions for Particles with Spin.Ann. Phys.* **7**,404-428.

[35] A. Zichichi et al.(1962). *Proton-Antiproton Annihilation into Electrons, Muons and Vector Bosons.Nuovo Cimento* **XXIV**(1),170-180.

[36] G. P. Lepage and S. J. Brodsky(1980). *Exclusive processes in perturbative quantum chromodynamics.Phys. Rev. D* **22**(9),2157-2198.

[37] P. Kroll, T. Pilsner, M. Schürmann and W. Schweiger(1993). *On exclusive reactions in the time-like region. Phy Lett. B* **316**,546-554.

[38] T. Gousset and B. Pire(1995). *Timelike form factors at high energy.Phys. Rev. D* **51**(1),15-24.

[39] G. Sterman and P. Stoler(1997). *Hadronic Form Factor and Perturbative QCD.Annu. Rev. Nucl. Part. Sci.* **47**,193-233.